Journal of Materials Chemistry C

Structural designs for ratiometric temperature sensing with organic fluorophores

Journal:	*Journal of Materials Chemistry C*
Manuscript ID	TC-REV-02-2019-000993.R1
Article Type:	Review Article
Date Submitted by the Author:	26-Mar-2019
Complete List of Authors:	Mazza, Mercedes; University of Miami, Chemistry Raymo, Francisco; University of Miami, Chemistry

Journal of Materials Chemistry C

REVIEW

Structural designs for ratiometric temperature sensing with organic fluorophores

Received 20th February 2019,
Accepted 5th April 2019

DOI: 10.1039/#

www.rsc.org/materials-c

Mercedes M. A. Mazza and Françisco M. Raymo*

The need to map temperature distributions at the micrometer level in a diversity of samples is stimulating the develpment of thermosensitive organic fluorophores with dual emission. Their ability to provide pairs of output signals simultaneously offers the opportunity to probe temperature ratiometrically and overcome the concentration effects and optical artifacts that plague methods based on single emission. Pronounced modifications in structure with temperature are generally invoked to ensure such a ratiometric response. Indeed, conformational changes in either the excited state or the ground state can be exploited to contruct thermosenstive molecular, macromoleuclar and supramolecular systems. Alternatively, the rapid equilibration of two fluorophores with resolved emisisons can be designed around the opening and closing of heterocyclic rings to impose, once again, ratiometric response. The behavior of these thermosensitive constructs in conjunction with the fast response time, inherent sensitivity, noninvasive character and spatial resolution of fluorescence imaging permits thermometric analyses at dimensional scales that cannot be accessed with conventional thermometers.

1. Introduction

Temperature is a crucial physical parameter that affects the behavior of diverse biological and chemical systems as well as numerous man-made and naturally-occurring materials.[1,2] These profound implications in biology, chemistry and materials science have sparked significant interest in the development of thermometric methods able to measure variations in temperature at the sub-microscale level over the last two decades.[3] In fact, conventional thermometry becomes ineffective when the size of the specimen under investigation is reduced to the sub-micrometer level and when high spatial resolution is required, such as in a number of biotechnological applications, microfluidics, microelectronics and micro-optics.[3,4] For example, the need to map intracellular temperature in living cells, where the interplay of exothermic and endothermic reactions regulate activity, demands thermometric measurements at the microscale.[5–7] Indeed, temperature fluctuations are associated with particular cellular pathogenesis of disease (*e.g.*, cancer).[8–10]

Thermometric methods are generally divided into contact (*i.e.*, thermocouples) and non-contact techniques. Protocols based on contact require the installation of a physical sensor on or within the sample (invasive) and, as a consequence, they cannot detect temperature within small areas or in different spots simultaneously. Non-contact methods are non-invasive (or semi-invasive) and offer many advantages, such as the possibility to detect simultaneously temperature changes over a sample characterized by a non-uniform temperature profile.[11] Among the latter category, optical sensors based on absorption, emission or Raman scattering have attracted significant attention and, in particular, fluorescence-based methods (both spectroscopic and imaging protocols) are emerging as the most promising for microthermometry.

Numerous thermo-responsive luminescent probes, based on either emissive inorganic compounds or fluorescent organic systems, have been developed over the past two decades.[12,13] They can be divided

Laboratory for Molecular Photonics, Departments of Biology and Chemistry, University of Miami, Coral Gables, USA. E-mail: fraymo@miami.edu.

into two wide categories based on their output signals: single or dual emission. The first category includes fluorescent molecular thermometers that rely on absolute-intensity changes of a single emission band. As a result of the single output, the detected signal can be affected significantly by several factors, such as the concentration of the fluorophore, the power of the excitation laser, the inhomogeneity of the fluorescent-probe distribution and the sensitivity of the detector. Some of these complications can be overcome with lifetime measurements, if the luminescence decay of the probe is designed to be temperature dependent.[14,15] Alternatively, intensity measurements on fluorescent probes with thermosensitive dual emission can circumvent these undesired effects by allowing the ratiometric comparison of two independent signals.[12,13] This particular class of thermoresponsive probes are the primary focus of this review. Specifically, the fundamental principles behind the design of organic molecules with ratiometric response to temperature are illustrated through representative examples categorized in five sub-groups differing in photophysical and/or structural properties.

2. Excitation dynamics of organic fluorophores

Organic fluorophores generally comprise functional groups with an extended π-system.[16,17] This structural feature allows for the absorption of photons in the ultraviolet and visible regions of the electromagnetic spectrum. Upon absorption of radiation, the electronic configuration of the fluorophore changes and its energy increases to populate one of the accessible excited states (*e.g.*, S_2 in Fig. 1). The excited species relaxes to the lowest singlet excited state (S_1 in Fig. 1) and then decays either radiatively to produce fluorescence or nonradiatively to release heat back to the ground state (S_0 in Fig. 1). The rate constant for fluorescence (k_F) and that for nonradiative decay (k_{NR}) ultimately dictate the fluorescence quantum yield (ϕ), according to equation (1). Both constants can vary significantly, relative to each other, with modifications in the environment around the fluorescent species. Thus, any thermally-induced alteration of the medium immediately around a given fluorophore can result in a change of k_F relative to k_{NR} and, hence, in either an increase or a decrease of ϕ, offering the opportunity to impose temperature sensitivity on the fluorescence intensity.

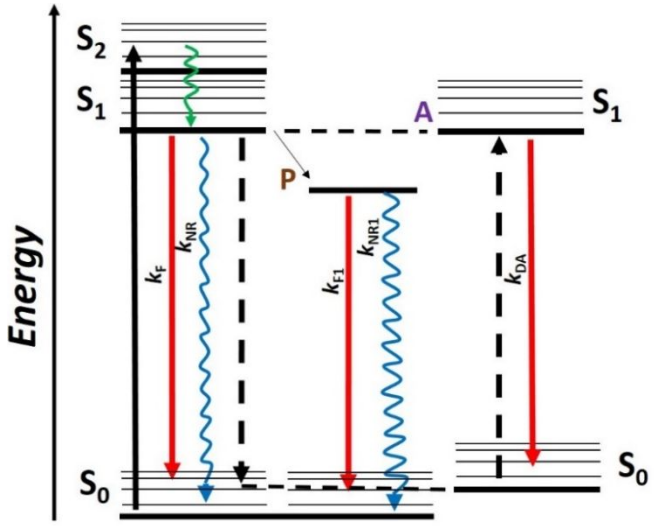

Fig. 1 Photophysical processes governing the excitation dynamics of organic fluorophores.

$$\phi = \frac{k_F}{k_F + k_{NR}} \quad (1)$$

The radiative and nonradiative pathways responsible for bringing an excited fluorophore from S_1 back to S_0 can be designed to compete with an additional temperature-sensitive process.[16,17] Specifically, a conformational change along the potential energy surface of S_1 can produce a new emissive species with different radiative and non-radiative rate constants (k_{F1} and k_{NR1}) relative to the original emitter (P in Fig. 1). The rate constant for such a change in molecular geometry can be very much sensitive to the viscosity of the medium, which in turn varies with temperature. Therefore, a change in temperature can ultimately translate into a change in fluorescence intensity under these conditions. Alternatively, the process competing with radiative and nonradiative decays can be the

transfer of energy from the excited fluorophore to a complementary acceptor (A in Fig. 1). The rate constant (k_{DA}) of energy transfer decreases with the sixth power of the distance separating donor and acceptor. Therefore, any mechanism capable of imposing thermal sensitivity on the physical separation between the two species exchanging energy translates into a temperature-induced change in the fluorescence intensity of the excited donor.

The intensity (I) of the radiation emitted by a solution of fluorescent molecules is related to ϕ, the intensity (I_0) of the exciting radiation as well as to the absorbance (A) of the sample, according to equation (2).[16,17] In turn, A depends linearly on the molar absorption coefficient (ε) and concentration (c) of the fluorescent species as well as the optical path length (d), according to equation (3). It follows that the fluorescence intensity changes with the concentration of the sample. Thus, any thermally-induced process designed to produce the fluorescent species (increase in c) or convert it into a different compound (decrease in c) can be exploited to impose temperature sensitivity on the detected fluorescence.

$$I = \phi\, I_0(1 - 10^{-A}) \quad (2)$$

$$A = \varepsilon\, c\, d \quad (3)$$

3. Twisted intramolecular charge transfer

The term twisted intramolecular charge transfer (TICT) was coined by Grabowski in his fundamental contributions[18] to the rationalization of the double fluorescence of compounds with bridged and sterically-hindered diethylamino groups.[19,20] TICT is a recurrent phenomenon in molecules incorporating pairs of subunits, connected through a single bond, that can act as electron donor (D) and acceptor (A) respectively upon excitation.[21] In the ground state, D and A adopt preferentially a co-planar arrangement to form a single chromophoric system with extended electronic conjugation. Vertical excitation produces a locally-excited (LE) state with the very same relative orientation of D and A. Once formed, the LE state can decay radiatively back to the ground state to produce fluorescence. Alternatively, it can undergo adiabatically a conformational change about the single bond connecting D and A to twist them out of planarity. Charge, in the form of an electron, is then transferred from D to A within the resulting twisted geometry, hence called TICT state. The latter can also deactivate radiatively to produce a weak emission that is generally red-shifted relative to the LE fluorescence.[16] The rate of the adiabatic conformational change varies significantly with the polarity and viscosity of the surrounding medium as well as with the temperature of the specimen. As a result, the relative amounts of the LE and TICT states and, therefore, their emission intensities change with any of these three physical parameters.[22,23] However, the emission bands of the LE and TICT states generally overlap significantly and the fluorescence quantum yield of the latter species is low in most instances.[19,24] These limitations complicate the development of compounds with ratiometric fluorescence response to temperature based of this particular mechanism.

In 2017, our laboratories reported a study on the structural implications on the excitation dynamics of fluorescent 3*H*-indolium cations.[25] Our investigations revealed that the excitation of compound IN (Fig. 2a) in acetonitrile populates efficiently a weakly-emissive TICT state. This molecule has a [C–C=C–C] bridge connecting a 3*H*-indolium cation to a coumarin chromophore. Fast rotation about the [C–C] bond adjacent to the coumarin fragment in the excited state is responsible for the formation of the TICT state.

The hexafluorophosphate salt of IN absorbs at 573 nm and the emission of its TICT state is centered at 640 nm in acetonitrile at 25 °C (Fig. 2b). Under these conditions, the fluorescence quantum yield (ϕ) is only 0.09 and the fluorescence decay is monoexponential with a lifetime (τ) of 0.31 ns. In viscous environments, rotation of the

coumarin fragment about the adjacent [C–C] bond slows down significantly, inhibiting the population of the TICT state. Indeed, ϕ is as high as 0.74 in glycerol at the same temperature and the decay is biexponential with a long component of 1.84 ns (63%) and a short one of 0.51 ns (37%). Singular-value decomposition of the time-resolved emission spectra clearly shows that the two components are associated with distinct emission bands with maxima at ~620 and ~650 nm (Fig. 2c), which correspond to the LE and TICT states respectively.

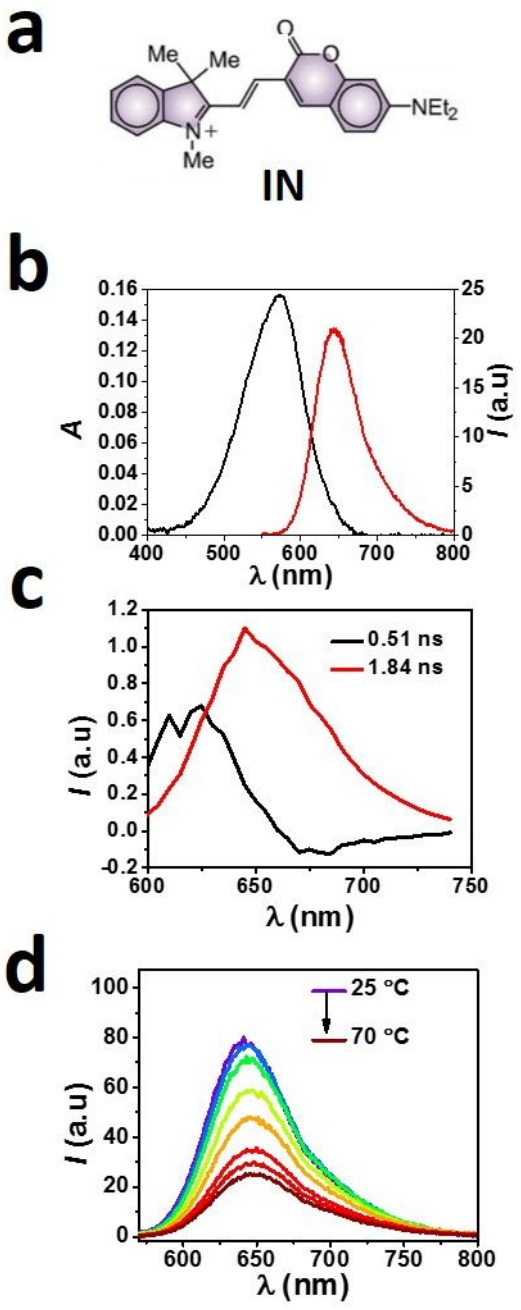

Fig. 2 (**a**) Structure of IN. (**b**) Absorption and emission spectra of the hexafluorophosphate salt of IN in acetonitrile at 25 °C. **(c)** Singular value decomposition of the time-resolved emission spectrum of the hexafluorophosphate salt of IN in glycerol at 25 °C. (**d**) Temperature dependence of the emission spectrum of the hexafluorophosphate sat of IN in glycerol/acetonitrile (94:6, v/v).

The temperature dependence of the emission spectrum was studied in a mixture of acetonitrile/glycerol (94:6, v/v) between 25 and 70 °C. A significant decrease in emission intensity was observed with a temperature increase (Fig. 2d). Indeed, the rate of the conformational change responsible for the adiabatic conversion of the LE into the TICT state increases with temperature. As a result, the population of the weakly-emissive TICT state is facilitated and the overall emission intensity decreases. However, the emission bands of the two emissive species overlap significantly and only after deconvolution (Fig. 2c) can be distinguished, complicating the possible implementation of a ratiometric detection scheme based on this compound.

4. Molecular beacons

Molecular beacons (MBs) were reported for the first time in 1995, when Tyagi and Kramer applied a new principle to construct probes able to detect specific nucleic acids in homogeneous solutions.[26] The general structure of MBs (Fig. 3) consists of a single-stranded nucleic acid with a stem-and-loop unit together and an overall hairpin shape.[26–30] Two complementary arm sequences, annealed together to form the stem, are connected through an additional probe sequence at one end. At the other, each arm is bound to a

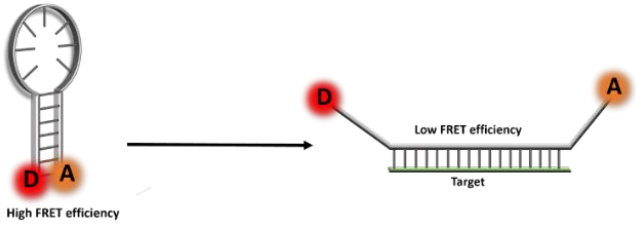

Fig. 3 Association of a MB with its complementary target separates D from A to depress the efficiency of FRET.

chromophoric group designed to act as energy donor (D, emissive) and acceptor (A, non-emissive) respectively in a Förster resonance energy transfer (FRET) pair.[31,32] These two moieties are maintained in close proximity by the stem, causing the fluorescence of D to be quenched by A though a FRET mechanism. Association of the probe to a complementary nucleotide promotes the formation of a probe–target complex, forcing the two arm sequences (as well as the appended D and A) to move away from each other and preventing FRET. The overall result is the restoration of the fluorescence of D.[33,34]

MBs undergo a conformational change upon heating with a resulting increase in fluorescence, which follows a sigmoidal trend.[35] MBs sensitivity to temperature has been largely used to design biocompatible fluorescent temperature sensors.[36–38] However, most of these probes are based on single emission.[36,39] In addition to the inherent disadvantages associated with the detection of a single output signal, they also have a range of action restricted to the melting temperature of the stem and are sensitivity to other chemical and physical parameters (*e.g.*, concentration, pH and viscosity).[36] In order to overcome these disadvantages, unimolecular dual-emission MBs sensitive to temperature have been designed. One explored strategy has been to substitute the non-emissive A, linked to one arm, with a fluorophore that can emit at its characteristic wavelength following FRET.[40] In 2009 Barilero *et al.* reported a dual-emission temperature sensor MB based on a Fluorescein/Texas-Red FRET pair designed to produce A or D fluorescence depending on temperature.[41] Indeed, their probe can adopt predominantly two distinct geometrical arrangements. In the closed state, FRET occurs and A emits. In the open state, FRET does not occur and D emits. After estimation of an optimal Föster distance of 5.6 nm, the authors engineered an oligonucleotide combining a loop long enough to obtain a significant increase of the average D–A distance and two complimentary sequences to form a stem with melting temperature around 20–25 °C.[42] Negligible temperature dependence was observed in the corresponding absorption spectra, showing bands for Fluorescein and Texas-Red centered at 495 and 594 nm respectively. The emission spectra of this MB, recorded in buffer solution upon excitation at the Fluorescein absorption wavelength, reveals two well distinguished emission bands corresponding to Fluorescein (518 nm) and Texas-red (610 nm) with the intensity of the former increasing and that of the latter decreasing to give a change in ratio (I_{518}/I_{610}) from ~0.47 to ~2.25, as the temperature increases from 7.3 to 36.5 °C. This ratiometric MB was tested in a 130-μm thick microfluidic chamber, locally heated by a thin-film resistor, obtaining maximum relative sensitivity at 20 °C.

A modified MB structure (Fig. 4a), consisting of a single-stranded DNA (ssDNA) terminated by a FRET pair, was reported by Wu *et al.* in 2017.[43] The absence of the double-stranded stem, characteristic of MBs, avoids the main disadvantage arising from the interaction between the nucleobases of the stem: *i.e.*, the thermally-induced formation and breaking of hydrogen bonding with a resulting working range limited to the melting temperature of the stem. In spite of these modifications, this probe retained the main function of traditional MBs. In fact, the conformation of certain ssDNA are temperature sensitive and this behavior is highly sequence-dependent.[44–46] Molecular dynamics simulations were used to investigate the thermosensitivity of a series of ssDNA sequences and 12-mers with lengths ranging between 3 and 6 nm, which are also compatible with FRET, were found to exhibit greater average sensitivities relative to 6-mer sequences. Steady-state fluorescence experiments at temperature ranging from 0 to 100 °C on 12-mer and 6-mer probes confirmed a conformational temperature-dependent

change in the former (Fig. 4b) and no significant sensitivity in the latter. In particular, a 12-mer with a phosphoramidites of 6-carboxyfluorescein (FAM) energy donor and a carboxy-tetramethyl-rhodamine (TAMRA) energy acceptor exhibited the largest temperature-dependent variation in the ratio between the emission intensities of D and A (corresponding to a decrease in FRET efficiency), ranging from 0.29 to 2.03 between 0 and 100 °C.

A similar probe, L-FAM-12R1-TAMRA, was tested as ratiometric temperature probe in biological applications. Laser scanning confocal microscopy images (LSCM) (Fig. 4c, A1–C3) of transfected PC-3 cells clearly demonstrate that signal intensities recorded in the D and A channels change ratiometrically with temperature. A related 12-mer probe, with a carboxy-X-rhodamine (ROX) energy donor and an ATTO 647N energy acceptor, was used to image the temperature change in a hyperthermia treatment of tumor tissue.[47–50] *In vivo* fluorescence images (Fig. 4c, D1–E2) of the tumor in a mice, recorded before and after hyperthermia, showed a significant change in the ratio between the emission intensities of D and A from 0.75 to 0.95 with hyperthermia.

5. Covalent blends of fluorophores

Most of the small-molecule thermosensors developed so far suffer from poor water solubility, limited possibility for functionalization and low structural stability.[13] Some of these major drawbacks can be overcome with the design of appropriate stimuli-responsive polymeric assemblies.[50–52] One viable strategy to construct fluorescent and temperature-sensitive polymers is based on the covalent connection of emissive chromophores to thermoresponsive macromolecules.[53–61] These particular macromolecules undergo a thermally-induced change in shape, which can affect the photophysical properties of the covalently-attached fluorophores.[6,58,62,63] Their covalent attachment to two or more types of fluorescent dyes further allows to engineer ratiometric response to temperature.[2,54,64–69]

In 2011, Chen *et al*. reported a molecular thermometer with ratiometric output based on co-polymerized units of *N-i*-propylacrylamide (NIPAM), *N,N'*-methylenebisacrylamine (MBAM), and 3-hydroxyflavone (3HF).[70] The emission of the 3HF component is sensitive to the polarity of the surrounding environment, because of the participation of normal excited-state intramolecular charge transfer (ESICT) and tautomer excited-state intramolecular proton transfer (ESIPT) in its excitation dynamics. Specifically, it emits at ~525 nm in polar aprotic solvents and ~425 nm in apolar protic solvents, because of the suppression of ESIPT under the latter conditions. The NIPAM-MBAM-3HFs co-polymer dispersed in

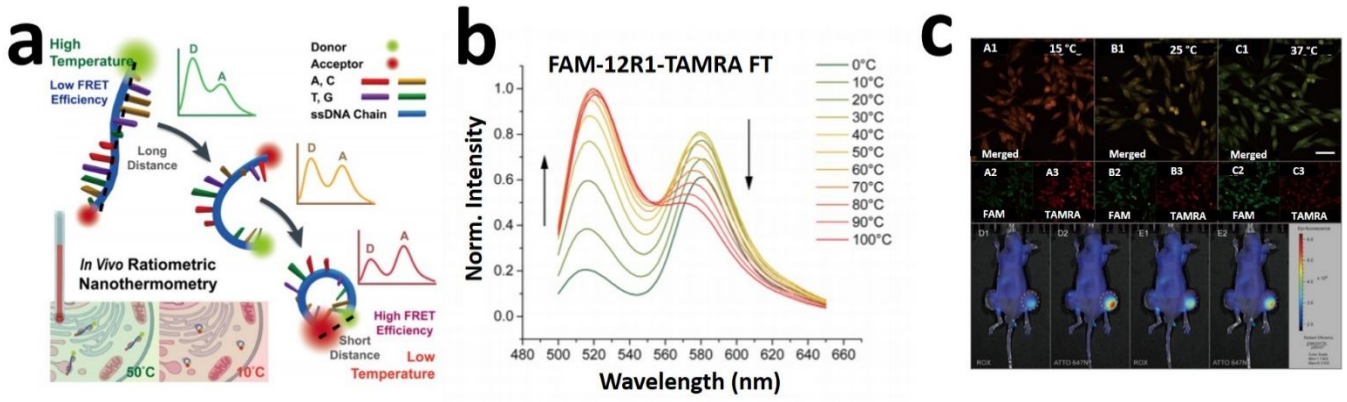

Fig. 4 (**a**) Schematic representation of a single-stranded DNA nanothermometer with ratiometric response based on FRET. (b) Temperature dependent emission of the FAM-12R1-TAMRA probe. (**c**) LSCM imaging of PC-3 cells transfected with the L-FAM-12R1-TAMRA probe at three different temperatures (A1–C3) and fluorescence imaging of tumor tissue injected with L-ROX-12R1-ATTO-FT before (D1 and D2) and after (E1 and E2) microwave irradiation. Reproduced from ref. 41 with permission (American Chemical Society).

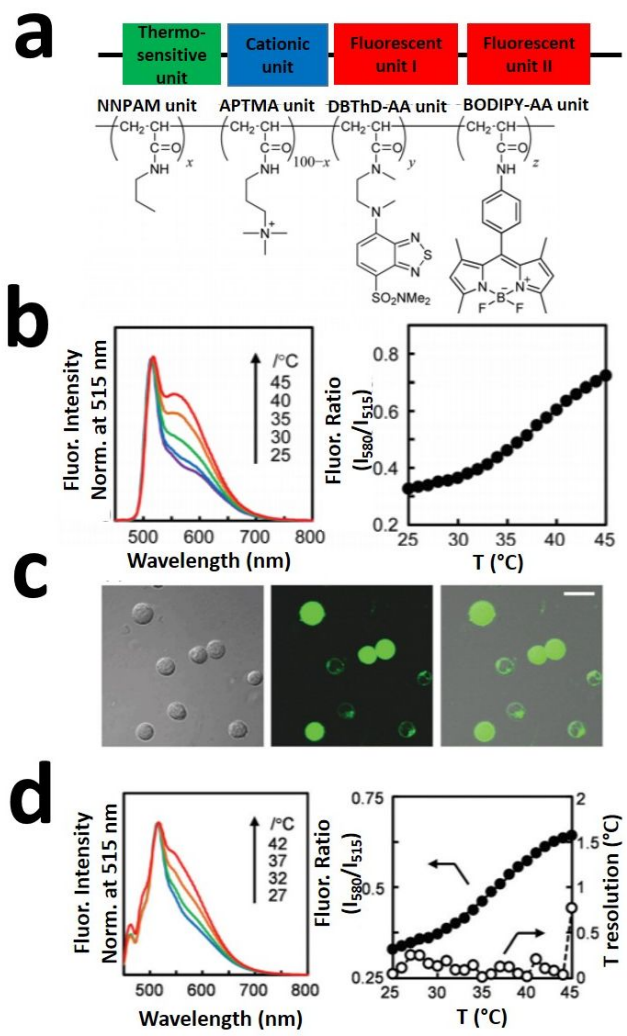

Fig. 5 (**a**) Structure of the cationic fluorescent polymeric thermometer composed of thermosensitive (NNPAM), cationic (APTMA), temperature dependent fluorescent (DBThD-AA) and temperature independent fluorescent (BODIPY-AA) units. (**b**) Normalized emission spectra of the cationic polymeric fluorescent probe recorded at different temperatures in aqueous KCl (150 mM, left) and the corresponding ratiometric change (right). (**c**) Differential interference contrast image (left), LSCM image (center) and merged images (right) of MOLT-4 cells incubated with the cationic fluorescent polymeric thermometer. (**d**) Emission spectra of MOLT-4 cells incubated with the polymeric thermometer (left) and the corresponding ratiometric change (right). Reproduced from ref. 69 with permission (Royal Society of Chemistry).

aqueous media adopts a swollen state below and a shrunk state above its lower critical solution temperature (LCST). These transformations are accompanied by significant changes in the ratio between the emission intensities at the two wavelengths. In particular, the I_{525}/I_{425} ratio shows a linear increase from ~0.1 to ~0.8 as the temperature raises from 33 and 41 °C. Furthermore, the modular design of this thermosensitive macromolecular constructs allows for the introduction of additional emissive components.[71]

In 2015, Uchiyama *et al.* designed a polymeric fluorescent thermometer based on poly-*N*-propylacrylamide (PNNPAM),[71] which undergoes a pronounced geometrical change, from linear to globular, as the temperature increases. In particular, PNNPAM is soluble in water below a lower critical solution temperature (LCST) of 10 °C.[72] This macromolecule was connected to a cationic unit ((3-acryl-amidopropyl) trimethylammonium salt (APTMA) to allow intracellular permeability,[73] a temperature-dependent benzothiadiazole (DbThD-AA) fluorophore[74] and a temperature independent borondipyrromethene emitter (BODIPY-AA) (Fig. 5a). The fluorescence of the temperature-sensitive DbThD-AA unit at 580 nm responds to variations in local polarity, caused by conformational changes of the PNNPAM backbone. A temperature raise from 25 to 45 °C produced an increase in the emission intensity of the DbThD-AA units, while that of the standard BODIPY-AA chromophores at 515 nm remained constant (Fig. 5b). As a result, the ratio between the two emission intensities (I_{580}/I_{515}) changed from ~0.3 to ~0.7 (Fig.5b, right), while variations in ionic strength (0.25–0.35), concentration (0.001–0.01 w/v %) and pH (6–9) did not show any significant effect. Non-adherent MOLT-4 (Fig. 5c) and adherent HEK293T cells were used to test incorporation efficiency, cytotoxicity and intracellular temperature sensitivity of this macromolecular probe. The fluorescence response to temperature was evaluated spectroscopically in multiple cells to give a change in I_{580}/I_{515} from ~0.10 to ~0.62 and from ~0.9 to ~1.3 in MOLT-4 and HEK293T cells respectively for temperatures ranging between 25 and 44 °C (Fig. 5d).

6. Noncovalent blends of fluorophores

The synthetic challenges associated with the need to attach multiple and distinct fluorophores to the same polymer backbone can be overcome with the engineering of noncovalent counterparts of these

macromolecular assemblies.[75–78] For example, a two-step cascade FRET temperature sensor was developed by Hu *et al.* in 2015.[79] Three different thermoresponsive fluorescent macromolecules, based on polyethylene glycol (PEG) and NIPAM polymers as well as coumarin (CMA), 7-nitro-1,2,3-benzoxadiazole (NBDA) and rhodamine B (RhBEA) fluorophores, were prepared (Fig. 6a). Each fluorophore was attached to a distinct polymer chain and the resulting macromolecules, emitting blue, green and red light respectively (Fig. 6b, left), were mixed. Thermo-induced micellization of the polymers in aqueous solution forced the attached fluorophores to be in close proximity, enabling FRET. The temperature response of the two-step cascade FRET ratiometric system was tested between 20 and 44 °C. An increase in FRET efficiency from CMA (λ_{EM} = 422 nm), trough NDB (λ_{EM} = 523 nm) to RhBEA (λ_{EM} = 585 nm) was observed with a raise in temperature. Specifically, the ratio between the emission intensities at 583 and 422 nm increased from ~1.5 to ~8.5 with a temperature change from 32 to 44 °C (Fig. 6b, right). Fluorescence images (Fig. 6c) of live HepG2 treated with an aqueous mix of the three polymers were successfully acquired in the corresponding detection channels (blue, green and red) at temperatures ranging from 25 to 41 °C, confirming the efficiency of the two-step cascade FRET mechanism. At temperatures below 33 °C, a strong blue emission was observed along with minimal red fluorescence. As the temperature was raised up to 41 °C, a dramatic increase of emission in the red channel was observed together with a decrease of that in the blue channel. The ratio between the emission intensities (I_{Red}/I_{Blue}) increased from ~1 to ~8 between 27 and 42 °C (Fig. 6d).

A more recent example of ratiometric temperature sensor, based on noncovalent blends of fluorophores, relies on the self-assembly of small amphiphilic building blocks. In particular, Cui *et al.* developed a new type of fluorescent nanoparticles through the self-assembly of amphiphilic small molecules, comprising a hydrophobic dicyanodistyrylbenzene (DCS) rod segment and hydrophilic oligo (ethylene glycol) OEG chains, in aqueous environments (Fig. 7a).[80] The OEG–DCS molecules displayed temperature responsive LCST behavior (Fig. 7b) similarly to that of the PNIPAM polymers. A shift of the emission maximum from 600 to 540 nm was observed in water

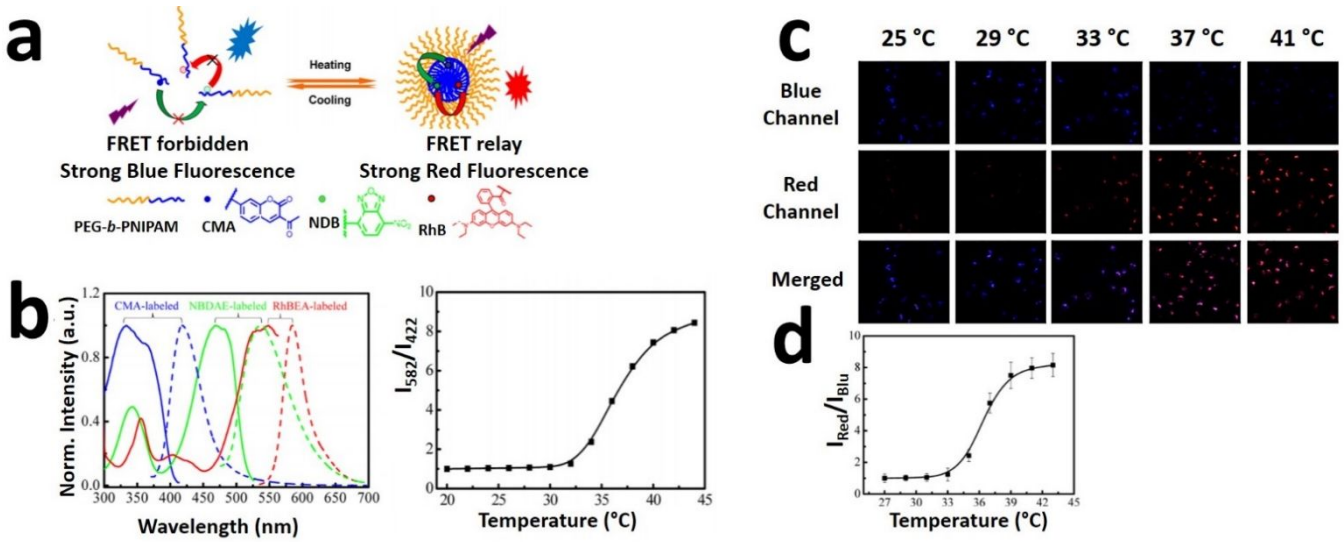

Fig. 6 (**a**) Schematic representation of a non-covalent blend of three fluorescent thermoresponsive hydrophilic block copolymers (PEG-*b*-PNIPAM-CMA, PEG-*b*-PNIPAM-NBD and PEG-*b*-PNIPAM-RhB) and the associated temperature-dependent FRET cascade. (**b**) Excitation (solid lines) and emission spectra (dotted lines) of the three polymers (left) and the corresponding ratiometric change (right). (**c**) LSCM images and associated ratiometric change (**d**) for live HEPG2 cells incubated with a mixture of the three polymers. Reproduced from ref. 76 with permission (American Chemical Society).

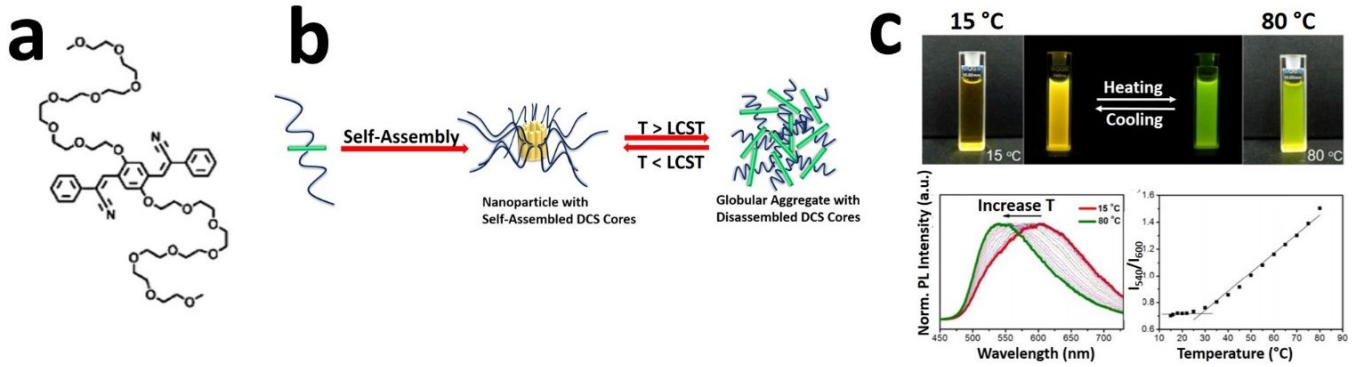

Fig. 7 (**a**) Structure of the OEG–DCS amphiphilic molecule. (**b**) Schematic representation of the reversible self-assembly (L < LCST) and disassembly (L > LCST) of OEG-DCS. (**c**) Color change of a solution containing OEG–DCS upon heating or cooling (top), normalized emission spectra of OEG–DCS at different temperatures (bottom left) and corresponding ratiometric response (bottom right). Reproduced from ref. 77 with permission (American Chemical Society).

with a raise in temperature from 15 (below the LCST) to 80 °C (Fig. 7c, bottom left). At low temperature, the hydrophilic OEG chains of the amphiphilic compounds interact with the surrounding water molecules to form hydrogen bonds. As the temperature increases above the LCST of OEG (26 °C) and then up to 80 °C, the hydrogen bonds are disrupted to form globular aggregates instead. Concomitantly with these structural changes, a linear increase in the ratio between the emission intensity of DCS globular aggregates at 540 nm and that of DCS self-assembled nanoparticles at 600 nm from ~0.7 to ~1.5 was observed for temperature above 26 °C (Fig. 7c, bottom right).

7. Thermochromic switches

The inherent sensitivity of thermochromic compounds[81,82] to temperature offers the opportunity to design fluorescent sensors with ratiometric response. Indeed, these particular molecules switch between states with resolved absorption bands in the visible region of the electromagnetic spectrum. As a result, significant changes in color accompany temperature-induced variations in the relative amounts of the two interconverting species. In principle, ratiometric fluorescence response to temperature can be engineered around these reversible transformations, if the two interconverting species are also designed to emit in resolved spectral regions. On the basis of these considerations, our laboratories developed fluorescent thermochromic switches based on the opening and closing of either oxazine or oxazolidine heterocycles.[83] Compound OX (Fig. 8a) is a representative example of these operating principles in action. It incorporates an oxazolidine heterocycle and a coumarin fluorophore. The two fragments are isolated electronically in the ground state and

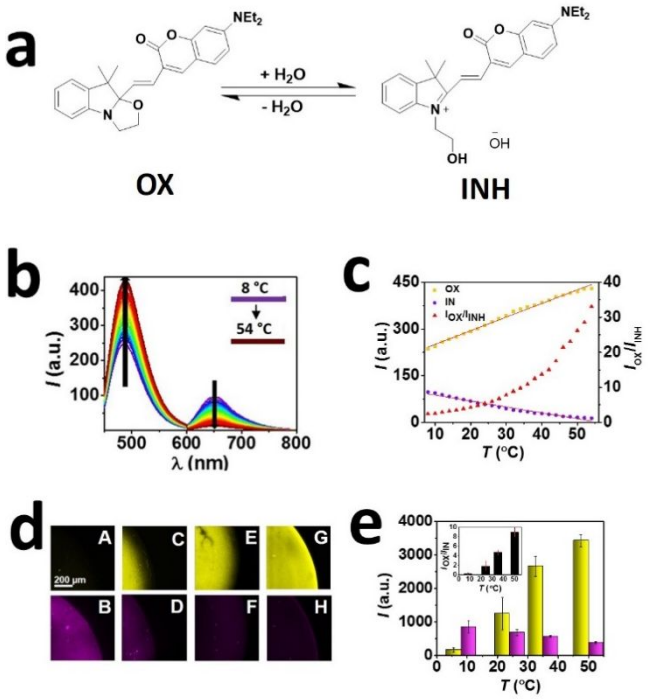

Fig. 8 (**a**) Interconversion of the ring-closed (OX) and -open (INH) forms of a thermochromic switch. (**b**) Emission spectra of OX and INH in MeCN/H_2O (1:1 v/v) at temperature ranging from 8 to 54 °C. (**c**) Temperature dependence of the emission intensities of OX and INH as well as of their ratio. (**d**) LSCM images of an alginate bead (diameter = 1.6 mm), doped with OX and maintained at 8 (A and B), 24 (C and D), 35 (E and F) or 50 °C (G and H) together with the corresponding emission intensities, integrated across the field of view, and their ratio (inset) [Yellow Channel: λ_{Ex} = 405 nm, λ_{Em} = 450–600 nm; Purple Channel: λ_{Ex} = 561 nm, λ_{Em} = 600–770 nm].

the fluorescent component emits at 489 nm. In a mixture of acetonitrile and water, however, the oxazolidine ring opens to form protonated indolium cation INH. In the resulting species, the coumarin fragment can extend its electronic conjugation over the adjacent indolium auxochrome to produce fluorescence at 660 nm. In fact, the emission spectrum (Fig. 8b) of an equilibrated solution of OX and INH clearly shows the resolved emission bands of the two species. As the temperature raises from 8 to 54 °C, the emission intensity of the ring-closed species increases and that of the ring-open form decreases. The ratio between the two intensities (Fig. 8c) also increases from ~2.4 to ~33 between 8 and 54 °C.

The observed ratiometric response of OX and INH was successful employed to image temperature distributions with spatial resolution at the micrometer level.[80] The thermochromic probe was entrapped within a hydrogel bead and the emission of the two equilibrating species was monitored at temperature ranging between 8 and 50 °C. The resulting images show an increase in the emission of OX (A, C, E and G in Fig. 8d) and a concomitant decrease in the emission of INH (B, D, F and H in Fig. 8d). A plot (Fig. 8e) of the ratio between the two emission intensities, integrated across the field of view, against temperature clearly reveal the ability of this molecular system to provide a ratiometric response with a change of I_{489}/I_{660} from 0.18 to 9 between 8 and 50 °C.

8. Conclusions

Fluorophores with electron rich and deficient fragments connected by a single bond can twist out of planarity upon excitation. The rate of such a conformational change and, hence, the relative amounts of excited molecules with planar and twisted geometries vary with temperature. As a result, these dynamic processes in the excited state provide a viable mechanism to design thermosensitive probes with dual emission. However, the overlap between the emission bands of the two species together with the low fluorescent quantum yield of the twisted state generally limit the performance of these systems.

Conformational changes in the ground state can also be exploited to control the relative intensities of pairs emission bands. In these systems, an energy donor is connected to an energy acceptor through a flexible spacer, whose geometry varies with temperature. As a result, the physical separation between donor and acceptor and, hence, the efficiency of energy transfer change significantly with temperature to affect the relative intensities of the emission bands of the two chromophoric components. However, the distance requirements that must be satisfied to suppress energy transfer demand the introduction of relatively long spacers between the two chromophoric components and restrict the implementation of these operating principles to macromolecular systems in most instances.

Blends of fluorophores with resolved emission bands covalently connected to either the same or distinct macromolecular backbones provide also the opportunity to implement ratiometric fluorescence response to temperature. Either conformational changes of the polymer scaffolds or their supramolecular association/dissociation in response to temperature alter the environment around the chromophoric units and, hence, their relative emission intensities. Once again, this design logic requires macromolecular scaffolds to ensure ratiometric response and cannot be scaled down to individual molecule-sized probes. Additionally, the phase transition of the polymer components restricts the temperature values that can be sensed within relatively narrow ranges.

Finally, the rapid equilibration of species with resolved emission bands, as a consequence of the opening and closing of heterocyclic rings, can also be exploited to ensure ratiometric response. Indeed, the relative amounts of two equilibrating compounds and, therefore,

the emission intensity of one relative to the other change significantly with temperature to provide ratiometric output. The main advantage of this particular approach is that it does not require the covalent connection to or noncovalent entrapment within a macromolecular construct and can, instead, be engineered into single organic molecules with appropriate structural designs, relying on the aid of chemical synthesis.

Each one of these valuable mechanisms, in conjunction with conventional fluorescence microscopes, offers the opportunity to visualize temperature distributions in a diversity of samples with spatial resolution at the micrometer level and in real time. In turn , their ratiometric response eliminates concentration effects and optical artifacts that, instead, complicate intensity measurements at a single wavelength. Thus, invaluable chemical thermometers for measurements at a dimensional scale that would be inaccessible to conventional thermometry can ultimately emerge from these innovative structural designs.

9. Acknowledgments

The National Science Foundation (CHE-1505885) is acknowledged for financial support.

10. Conflict of interest

There are no conflicts to declare.

11. References

1. X.-D. Wang, O. S. Wolfbeis and R. J. Meier, *Chem. Soc. Rev.*, 2013, **42**, 7834–7869.
2. F. Ye, C. Wu, Y. Jin, Y.-H. Chan, X. Zhang and D. T. Chiu, *J. Am. Chem. Soc.*, 2011, **133**, 8146–8149.
3. M. Quintanilla and L. M. Liz-Marzán, *Nano Today*, 2018, **19**, 126–145.
4. M. A. Bennet, P. R. Richardson, J. Arlt, A. McCarthy, G. S. Buller and A. C. Jones, *Lab on a Chip*, 2011, **11**, 3821–3828.
5. F. Vetrone, R. Naccache, A. Zamarrón, A. Juarranz de la Fuente, F. Sanz-Rodríguez, L. Martinez Maestro, E. Martín Rodriguez, D. Jaque, J. García Solé and J. A. Capobianco, *ACS Nano*, 2010, **4**, 3254–3258.
6. K. Okabe, N. Inada, C. Gota, Y. Harada, T. Funatsu and S. Uchiyama, *Nat. Commun.*, 2012, **3**, 705.
7. J. S. Donner, S. A. Thompson, M. P. Kreuzer, G. Baffou and R. Quidant, *Nano Lett.*, 2012, **12**, 2107–2111.
8. J. F. Head and R. L. Elliott, *Cancer*, 1997, **79**, 186–188.
9. H. J. Isard, *J. Am. Med Assoc.*, 1992, **268**, 3074–3074.
10. C. Stefanadis, C. Chrysohoou, D. B. Panagiotakos, E. Passalidou, V. Katsi, V. Polychronopoulos and P. K. Toutouzas, *BMC cancer*, 2003, **3**, 1.
11. P. Childs, J. Greenwood and C. Long, *Rev. Sci. Instrum.*, 2000, **71**, 2959–2978.
12. K. T. V. Grattan and Z. Y. Zhang in *Topics in Fluorescence Spectroscopy*, Ed. J. R. Lakowicz, Springer, New York, 2006, Vol. 4, pp. 335–376.
13. T. Qin, B. Liu, K. Zhu, Z. Luo, Y. Huang, C. Pan and L. Wang, *TrAC, Trends Anal. Chem.*, 2018, **102**, 259–271.
14. A. Steinegger, I. Klimant and S. M. Borisov, *Adv. Opt. Mater.*, 2017, **5**, 1700372
15. S. M. Borisov, R. Pommer, J. Svec, S. Peters, V. Novakova and I. Klimant, *J. Mater. Chem. C*, 2018, **6**, 8999–9009.
16. B. Valeur and M. N. Berberan-Santos, *Molecular Fluorescence: Principles and Applications*, John Wiley & Sons, 2012.
17. J. R. Lakowicz, *Principles of Fluorescence Spectroscopy*, Springer, New York, 2006.
18. Z. R. Grabowski, K. Rotkiewicz and A. Siemiarczuk, *J. Lumin.*, 1979, **18**, 420–424.
19. W. Rettig and E. A. Chandross, *J. Photochem.*, 1985, **28**, 351–366.
20. E. Lippert and W. Luder, *J. Phys. Chem.*, 1962, **66**, 2430–2434.
21. Z. R. Grabowski, K. Rotkiewicz and W. Rettig, *Chem. Rev.*, 2003, **103**, 3899–4032.
22. R. Hayashi, S. Tazuke and C. W. Frank, *Macromolecules*, 1987, **20**, 983–988.
23. S. Sasaki, G. P. Drummen and G.-I. Konishi, *J. Mater. Chem. C*, 2016, **4**, 2731–2743.
24. S. K. Saha, P. Purkayastha, A. B. Das and S. Dhara, *J. Photochem. Photobiol. A: Chem.*, 2008, **199**, 179–187.
25. E. R. Thapaliya, J. Garcia-Amorós, S. Nonell, B. Captain and F. M. Raymo, *Phys. Chem. Chem. Phys.*, 2017, **19**, 11904–11913.
26. S. Tyagi and F. R. Kramer, *Nat. Biotechnol.*, 1996, **14**, 303–308.
27. W. Tan, K. Wang and T. J. Drake, *Curr. Op. Chem. Biol.,* 2004, **8**, 547–553.
28. Y. Li, X. Zhou and D. Ye, *Biochem. Biophys. Res. Commun.*, 2008, **373**, 457–461.
29. K. Wang, Z. Tang, C. J. Yang, Y. Kim, X. Fang, W. Li, Y. Wu, C. D. Medley, Z. Cao and J. Li, *Angew. Chem. Int. Ed.*, 2009, **48**, 856–870.
30. J. Zheng, R. Yang, M. Shi, C. Wu, X. Fang, Y. Li, J. Li and W. Tan, *Chem. Soc. Rev.*, 2015, **44**, 3036–3055.
31. S. Jockusch, A. A. Martí, N. J. Turro, Z. Li, X. Li, J. Ju, N. Stevens and D. L. Akins, *Photochem. Photobiol. Sci.*, 2006, **5**, 493–498.
32. S. A. Marras, F. R. Kramer and S. Tyagi, *Nucleic Acids Res.*, 2002, **30**, e122.
33. P. Zhang, T. Beck and W. Tan, *Angew. Chem. Int. Ed.*, 2001, **40**, 402–405.
34. G. Bonnet, O. Krichevsky and A. Libchaber, *Proc. Natl. Acad. Sci. USA*, 1998, **95**, 8602–8606.
35. A. Dodge, G. Turcatti, I. Lawrence, N. F. de Rooij and E. Verpoorte, *Anal. Chem.*, 2004, **76**, 1778–1787.
36. G. Ke, C. Wang, Y. Ge, N. Zheng, Z. Zhu and C. J. Yang, *J. Am. Chem. Soc.*, 2012, **134**, 18908–18911.
37. S. Ebrahimi, Y. Akhlaghi, M. Kompany-Zareh and Å. Rinnan, *ACS Nano*, 2014, **8**, 10372–10382.
38. D. Gareau, A. Desrosiers and A. Vallée-Bélisle, *Nano Lett.*, 2016, **16**, 3976–3981.

39. A. T. Jonstrup, J. Fredsøe and A. H. Andersen, *Sensors*, 2013, **13**, 5937–5944.
40. J. Ueberfeld and D. R. Walt, *Anal. Chem.*, 2004, **76**, 947–952.
41. T. Barilero, T. Le Saux, C. Gosse and L. Jullien, *Anal. Chem.*, 2009, **81**, 7988–8000.
42. M. Zuker, *Nucleic Acids Res.*, 2003, **31**, 3406–3415.
43. Y. Wu, J. Liu, Y. Wang, K. Li, L. Li, J. Xu and D. Wu, *ACS Appl. Mater. Interf.*, 2017, **9**, 11073–11081.
44. F. W. Studier, *J. Mol. Biol.*, 1969, **41**, 189–197.
45. J. Ramprakash, B. Lang and F. P. Schwarz, *Biopolym.,* 2008, **89**, 969–979.
46. R. Ghirlando and G. Felsenfeld, *Biopolym.*, 2013, **99**, 910–915.
47. T. Bai and N. Gu, *Small*, 2016, **12**, 4590–4610.
48. D. Jaque and F. Vetrone, *Nanoscale*, 2012, **4**, 4301–4326.
49. B. del Rosal, E. Ximendes, U. Rocha and D. Jaque, *Adv. Opt. Mat.*, 2017, **5**, 1600508.
50. E. Y. Kim, D. Kumar, G. Khang and D.-K. Lim, *J. Mater. Chem. B.*, 2015, **3**, 8433–8444.
51. F. Liu and M. W. Urban, *Prog. Polym. Sci.*, 2010, **35**, 3–23.
52. M. A. C. Stuart, W. T. Huck, J. Genzer, M. Müller, C. Ober, M. Stamm, G. B. Sukhorukov, I. Szleifer, V. V. Tsukruk and M. Urban, *Nat. Mater.*, 2010, **9**, 101–113.
53. E. G. Bellomo, M. D. Wyrsta, L. Pakstis, D. J. Pochan and T. J. Deming, *Nat. Mater.*, 2004, **3**, 244–248.
54. O. Lavastre, I. Illitchev, G. Jegou and P. H. Dixneuf, *J. Am. Chem. Soc.*, 2002, **124**, 5278–5279.
55. H. Zhou, F. Liu, X. Wang, H. Yan, J. Song, Q. Ye, B. Z. Tang and J. Xu, *J. Mater. Chem. C*, 2015, **3**, 5490–5498.
56. S. Uchiyama, Y. Matsumura, A. P. de Silva and K. Iwai, *Anal. Chem.*, 2003, **75**, 5926–5935.
57. S. Uchiyama, Y. Matsumura, A. P. de Silva and K. Iwai, *Anal. Chem.*, 2004, **76**, 1793–1798.
58. C. Gota, K. Okabe, T. Funatsu, Y. Harada and S. Uchiyama, *J. Am. Chem. Soc.*, 2009, **131**, 2766–2767.
59. K. Iwai, Y. Matsumura, S. Uchiyama and A. P. de Silva, *J. Mater. Chem.*, 2005, **15**, 2796–2800.
60. M. Onoda, S. Uchiyama and T. Ohwada, *Macromolecules*, 2007, **40**, 9651–9657.
61. Y. Shiraishi, R. Miyamoto and T. Hirai, *Org. Lett.*, 2009, **11**, 1571–1574.
62. J. Qiao, X. Mu and L. Qi, *Biosens. Bioelectron.*, 2016, **85**, 403–413.
63. T. Tsuji, S. Yoshida, A. Yoshida and S. Uchiyama, *Anal. Chem.*, 2013, **85**, 9815–9823.
64. S. H. Lee, H. T. Bui, T. P. Vales, S. Cho and H.-J. Kim, *Dyes Pigm.*, 2017, **145**, 216–221.
65. C.-Y. Chen and C.-T. Chen, *Chem. Commun.*, 2011, **47**, 994–996.
66. J. Hu, X. Zhang, D. Wang, X. Hu, T. Liu, G. Zhang and S. Liu, *J. Mater. Chem.*, 2011, **21**, 19030–19038.
67. J. Qiao, C. Chen, L. Qi, M. Liu, P. Dong, Q. Jiang, X. Yang, X. Mu and L. Mao, *J. Mater. Chem. B*, 2014, **2**, 7544–7550.
68. D. Wang, T. Liu, J. Yin and S. Liu, *Macromolecules*, 2011, **44**, 2282–2290.
69. T. Wu, G. Zou, J. Hu and S. Liu, *Chem. Mater.*, 2009, **21**, 3788–3798.
70. C.-Y. Chen, C.-T. Chen, *Chem. Commun.*, 2011, **47**, 994–996.
71. S. Uchiyama, T. Tsuji, K. Ikado, A. Yoshida, K. Kawamoto, T. Hayashi and N. Inada, *Analyst*, 2015, **140**, 4498–4506.
72 S. Chen, K. Wang and W. Zhang, *Polym. Chem.*, 2017, **8**, 3090–3101.
73. C. Gota, S. Uchiyama and T. Ohwada, *Analyst*, 2007, **132**, 121–126.
74. S. Uchiyama, K. Kimura, C. Gota, K. Okabe, K. Kawamoto, N. Inada, T. Yoshihara and S. Tobita, *Chem. Eur. J.*, 2012, **18**, 9552–9563.
75. Y. Wu, J. Liu, J. Ma, Y. Liu, Y. Wang and D. Wu, *ACS Appl. Mater. Interf.*, 2016, **8**, 14396–14405.
76. T. Kan, H. Aoki, N. Binh-Khiem, K. Matsumoto and I. Shimoyama, *Sensors*, 2013, **13**, 4138–4145.
77. J. Liu, X. Guo, R. Hu, J. Xu, S. Wang, S. Li, Y. Li and G. Yang, *Anal. Chem.*, 2015, **87**, 3694–3698.
78. S. Inal, J. D. Kölsch, F. Sellrie, J. A. Schenk, E. Wischerhoff, A. Laschewsky and D. Neher, *J. Mater. Chem. B*, 2013, **1**, 6373–6381.
79. X. Hu, Y. Li, T. Liu, G. Zhang and S. Liu, *ACS Appl. Mater. Interf.*, 2015, **7**, 15551–15560.
80. J. Cui, J. E. Kwon, H.-J. Kim, D. R. Whang and S. Y. Park, *ACS Appl. Mater. Interf.*, 2017, **9**, 2883–2890.
81. J. C. Crano and Guglielmetti (eds.), *Organic Photochromic and Thermochromic Compounds,* Plenum Press, New York, 1999, **1**, 85.
82. J. H. Day, *Chem. Rev.*, 1963, **63**, 65–80.
83. M. M. Mazza, F. Cardano, J. Cusido, J. D. Baker, S. Giordani and F. M. Raymo, *Chem. Commun.*, 2019, **55**, 1112–1115.

Mercedes M. A. Mazza received a MS in Chemistry from the University of Cagliari (Italy) in 2014. She is currently a graduate student in the chemistry program of the University of Miami, working under the supervision of Professor Raymo. Her graduate research involves the design and characterization of stimuli-responsive molecular switches with applications in fluorescence imaging. She authored 7 publications in the general areas of fluorescence imaging, material science, molecular switches and photochemistry.

Françisco M. Raymo received a Laurea in Chemistry from the University of Messina (Italy) in 1992 and a Ph.D. in Chemistry from the University of Birmingham (UK) in 1996. He was a postdoctoral associate at the University of Birmingham (UK) in 1996–1997 and at the University of California, Los Angeles in 1997–1999. He was appointed Assistant Professor of Chemistry at the University of Miami in 2000 and promoted to Associate Professor in 2004 and Full Professor in 2009. His research interests combine the design, synthesis and analysis of switchable molecular constructs for imaging applications. He authored more than 250 publications.

Table of Contents

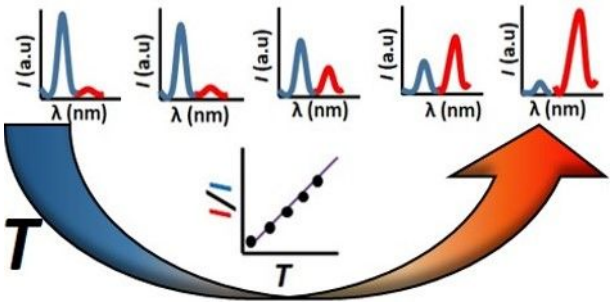

Thermosensitive probes with dual emission allow the ratiometric sensing of temperature with fluorescence measurements.